New class of turbulence in active fluids

Vasil Bratanov[a], Frank Jenko[b,1], and Erwin Frey[c]

[a]Tokamak Physics Division, Max Planck Institute for Plasma Physics, D-85748 Garching, Germany; [b]Department of Physics and Astronomy, University of California, Los Angeles, CA 90095; and [c]Arnold Sommerfeld Center for Theoretical Physics and Center for NanoScience, Department of Physics, Ludwig-Maximilians-Universität München, D-80333 Munich, Germany

Edited by Alexander J. Smits, Princeton University, Princeton, NJ, and accepted by the Editorial Board October 29, 2015 (received for review May 12, 2015)

Turbulence is a fundamental and ubiquitous phenomenon in nature, occurring from astrophysical to biophysical scales. At the same time, it is widely recognized as one of the key unsolved problems in modern physics, representing a paradigmatic example of nonlinear dynamics far from thermodynamic equilibrium. Whereas in the past, most theoretical work in this area has been devoted to Navier–Stokes flows, there is now a growing awareness of the need to extend the research focus to systems with more general patterns of energy injection and dissipation. These include various types of complex fluids and plasmas, as well as active systems consisting of self-propelled particles, like dense bacterial suspensions. Recently, a continuum model has been proposed for such "living fluids" that is based on the Navier–Stokes equations, but extends them to include some of the most general terms admitted by the symmetry of the problem [Wensink HH, et al. (2012) *Proc Natl Acad Sci USA* 109:14308–14313]. This introduces a cubic nonlinearity, related to the Toner–Tu theory of flocking, which can interact with the quadratic Navier–Stokes nonlinearity. We show that as a result of the subtle interaction between these two terms, the energy spectra at large spatial scales exhibit power laws that are not universal, but depend on both finite-size effects and physical parameters. Our combined numerical and analytical analysis reveals the origin of this effect and even provides a way to understand it quantitatively. Turbulence in active fluids, characterized by this kind of nonlinear self-organization, defines a new class of turbulent flows.

turbulence | active fluids | self-organization

Despite several decades of intensive research, turbulence—the irregular motion of a fluid or plasma—still defies a thorough understanding. It is a paradigmatic example of nonlinear dynamics and self-organization far from thermodynamic equilibrium also closely linked to fundamental questions about irreversibility (1) and mixing (2). The classical example of a turbulent system is a Navier–Stokes flow, with a single quadratic nonlinearity, well-separated drive and dissipation ranges, and an extended intermediate range of purely conservative scale-to-scale energy transfer (3). However, many turbulent systems of scientific interest involve more general patterns of energy injection, transfer, and dissipation. A fascinating example of these kinds of generalized turbulent dynamics can be observed in dense bacterial suspensions (4). Although the motion of the individual swimmers in the background fluid takes place at Reynolds numbers well below unity, the coarse-grained dynamics of these self-propelled particles display spatiotemporal chaos, i.e., turbulence (5–7). Nevertheless, the correlation functions of the velocity and vorticity fields display some essential differences compared with their counterparts in classical fluid turbulence (8, 9). Moreover, the collective motion of bacteria in such suspensions exhibits long-range correlations (10), appears to be driven by internal instabilities (11), and depends strongly also on physical parameters like large-scale friction (12). Such results challenge the orthodox understanding of turbulent motion and call for a detailed theoretical investigation. There also exist many other systems with similar characteristics, including flows generated by space-filling fractal square grids (13) , turbulent astrophysical (14) and laboratory (15, 16) plasmas, and chemical reaction–diffusion processes (17).

In the present work, we study—numerically as well as analytically—the spectral properties of a continuum model that has recently been suggested as a minimal phenomenological model to describe the collective dynamics of dense bacterial suspensions (4, 18, 19). A basic assumption of the model is that at high concentrations the dynamics of bacterial flow may be described as an incompressible fluid obeying the following equation of motion for the velocity field $\mathbf{v}(\mathbf{x},t)$,

$$\frac{\partial \mathbf{v}}{\partial t}+\lambda_0(\mathbf{v}\cdot\nabla)\mathbf{v}+\nabla p=-\Gamma_0\Delta\mathbf{v}-\Gamma_2\Delta^2\mathbf{v}-\mu(v)\mathbf{v}, \qquad [1]$$

where $\mu(v)=\alpha+\beta|\mathbf{v}|^2$. In addition to the advective nonlinearity, $(\mathbf{v}\cdot\nabla)\mathbf{v}$, and pressure term, ∇p, familiar from the Navier–Stokes model, the equation also accounts for internal drive and dissipation processes. Apart from the last term on the right-hand side and the pressure term, Eq. **1** amounts to a straightforward multidimensional generalization of the Kuramoto–Sivashinsky (KS) equation that has found application in describing magnetized plasmas (20, 21), chemical reaction–diffusion processes (22, 23), and flame front propagation (24, 25). It is widely regarded as a prototypical example of "phase turbulence." (26) As a hallmark, if both kinetic parameters are positive (Γ_0, $\Gamma_2>0$), the KS equation is linearly unstable for a band of wave vectors k, similar to other paradigmatic models of nonlinear dynamics, e.g., the Swift–Hohenberg model (27). For active systems this feature emulates energy input into the bacterial system through stress-induced instabilities (11). The growth of these linearly unstable modes is limited by nonlinear and dissipative terms. The main dissipation mechanism in Eq. **1** is mediated through the cubic nonlinearity on the right-hand side, $-\mu(v)\mathbf{v}$. Such a term was originally introduced by Toner and Tu to account for a propensity of self-propelled rod-like objects to exhibit local polar order ("flocking") (28, 29). This hydrodynamic model comprises some of the key features common to systems exhibiting mesoscale turbulence: interplay of energy input due to a band of linearly unstable modes with the advective

Significance

It is widely appreciated that turbulence is one of the main challenges of modern theoretical physics. Whereas up to now, most work in this area has been dedicated to the study of Navier–Stokes flows, numerous examples exist of systems that exhibit similar types of spatiotemporal chaos but are described by more complex nonlinear equations. One such problem of quickly growing scientific interest is turbulence in active fluids. We find that such systems can exhibit power-law energy spectra with nonuniversal exponents as a result of nonlinear self-organization, defining a new class of turbulent flows.

Author contributions: F.J. designed research; V.B., F.J., and E.F. performed research; and V.B., F.J., and E.F. wrote the paper.

The authors declare no conflict of interest.

This article is a PNAS Direct Submission. A.J.S. is a guest editor invited by the Editorial Board.

[1]To whom correspondence should be addressed. Email: jenko@physics.ucla.edu.

This article contains supporting information online at www.pnas.org/lookup/suppl/doi:10.1073/pnas.1509304112/-/DCSupplemental.

Navier–Stokes nonlinearity as well as with terms modeling flocking behavior and dissipation. These generic features are shared by more elaborate hydrodynamic models of active matter recently reviewed in ref. 30. Thus, Eq. **1** serves as a simple but generic test case to address some of the fundamental questions in the field of active turbulence. Via an appropriate choice of parameters, one can describe several different physical systems as explained in more detail in Table S1.

First and foremost, the similarities and differences between low and high Reynolds number turbulence remain to be elucidated. In particular, there is still a lack of understanding of the energy flow between different length scales. Here, we address the above questions by a systematic analysis of the turbulent features of Eq. **1**, combining numerical and analytical approaches, and we give a comprehensive picture of the spectral energy balance facilitating the understanding of the interactions among different spatial scales. Furthermore, extensive numerical simulations confirm the existence of a spectral power law at the largest scales of the system with its steepness depending on the parameters of the system (both of the linear and of the nonlinear terms in Eq. **1**). The form of the turbulent energy spectrum is an important quantity related to the frictional drag between the system and the surrounding walls (31, 32). In the present work, insight into the remarkable feature of a variable spectral exponent is gained by analyzing the role of the different terms in the equation for the spectral energy balance. As expected for a 2D incompressible fluid, there exists an inverse flow of energy from intermediate to large scales (33). Nevertheless, in contrast to classical, fully developed 2D Navier–Stokes turbulence, there is no inertial range characterized by a constant energy flux. Instead, we find that at large scales the nonlinear frequency corresponding to the Navier–Stokes energy flux is constant for the whole range characterized by spectral self-similarity. This differs fundamentally from the classical Navier–Stokes case, where this nonlinear frequency, the inverse of the nonlinear eddy turnover time, is a function of wave number and energy. In the model at hand, this energy flux is balanced by a linear dissipation/injection and a cubic dissipation term. For the latter, we derive an analytic approximation that compares very favorably with the numerical results and allows for an analytic closure predicting the type of dependence of the power law on the model parameters that is also confirmed numerically.

Results

We have studied the 2D version of the continuum model defined by Eq. **1** both analytically and numerically. Our computational approach relies on a pseudospectral code where the linear terms are computed in Fourier space and the nonlinearities in real space. The details of this procedure and the necessary normalization are described in *SI Text*, section S1. All numerical results reported in this paper use a resolution of 1,024 effective Fourier modes in each direction, unless stated otherwise. A typical velocity is given by $v_0 := \sqrt{\Gamma_0^3/\Gamma_2}$. From the spectral representation $\gamma(k) := -\alpha + \Gamma_0 k^2 - \Gamma_2 k^4$ of the linear part of Eq. **1**, one reads off the wave number of the fastest growing mode, $k_{\max} = \sqrt{\Gamma_0/(2\Gamma_2)}$, which suggests characteristic length and time scales as $\ell = 5\pi/k_{\max}$ and $\tau = \ell/v_0$, respectively. Accordingly, the normalized form of the parameters Γ_0 and Γ_2 reduces to fixed numbers; i.e., $\Gamma_0\tau/\ell^2 = 1/(5\sqrt{2}\pi)$ and $\Gamma_2/(\ell v_0^3) \approx 9\cdot 10^{-5}$. The parameters β and λ_0 can still be chosen freely and here they are set to $\beta\tau v_0 = 0.5$ and $\lambda_0 = 3.5$. The normalization units used here are the same as the ones in ref. 4, meaning that our parameters (with $\alpha = -1$ and up to the different sign of Γ_0) correspond to the bacterial suspension described therein. A typical snapshot of the real-space vorticity field in the turbulent regime is shown in Fig. 1. It makes evident the random distribution of vortices across the simulation domain. Moreover, the time evolution of the vortex configuration turns out to be strongly incoherent. Due to this highly nonlinear behavior, associated with spatiotemporal chaos, exhibited by the system, we refer to its dynamics as turbulent.

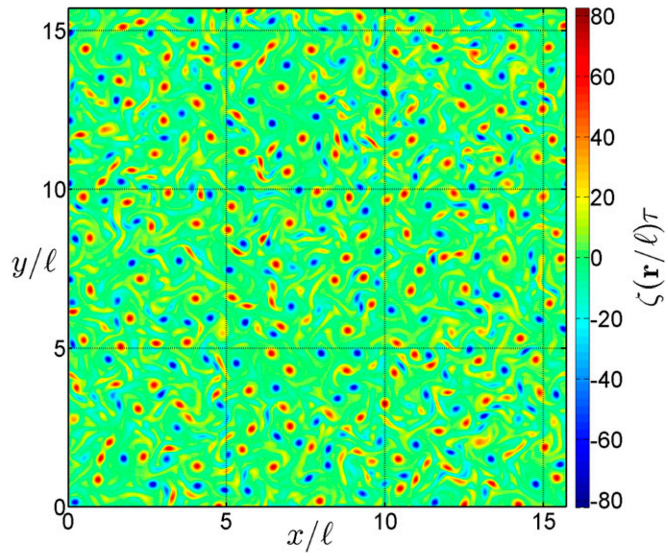

Fig. 1. Snapshot of the 2D vorticity field $\zeta = \partial_x v_y - \partial_y v_x$ right after the onset of the turbulent regime as obtained from a numerical solution of Eq. **1**, using a pseudospectral code. The computation has been performed with 1,024 (effective) points in each direction under the constraint of periodic boundary conditions. The Ekman parameter equals $\alpha\tau = -1$, implying that there are two energy sources acting at large scales—the two positive terms in the expression for $\gamma(k)$. The strength of the cubic nonlinearity is set to $\beta\tau v_0 = 0.5$ and for the advective term we have used $\lambda_0 = 3.5$. One can clearly see the highly disordered distribution of vortices justifying the classification of the regime as turbulent.

Spectral Analysis. For the analysis of the flow of energy between different spatial scales mediated by the various terms in Eq. **1** we use a Fourier decomposition of $\mathbf{v}$ (*SI Text*, section S1). $E_{\mathbf{k}} := \langle |\mathbf{v_k}(t)|^2 \rangle /2$ is referred to as the energy of Fourier mode $\mathbf{k}$, where $\langle \cdot \rangle$ denotes an ensemble average, equivalent to a time average for a statistically stationary state as discussed in *SI Text*, section S1. The ensuing spectral energy balance equation reads

$$\partial_t E_{\mathbf{k}} = 2\gamma(k) E_{\mathbf{k}} + T_{\mathbf{k}}^{\mathrm{adv}} + T_{\mathbf{k}}^{\mathrm{cub}}, \qquad [2]$$

with the advective and cubic nonlinear terms given by

$$T_{\mathbf{k}}^{\mathrm{adv}} = +\lambda_0 \ \mathrm{Re}\left[\sum_{\mathbf{p}} M_{ijl}(\mathbf{k}) \left\langle v_{-\mathbf{k}}^i v_{\mathbf{k}-\mathbf{p}}^l v_{\mathbf{p}}^j \right\rangle\right], \qquad [3a]$$

$$T_{\mathbf{k}}^{\mathrm{cub}} = -\beta \ \mathrm{Re}\left[\sum_{\mathbf{p},\mathbf{q}} D_{ij}(\mathbf{k}) \left\langle v_{-\mathbf{k}}^i v_{\mathbf{k}-\mathbf{p}-\mathbf{q}}^l v_{\mathbf{q}}^l v_{\mathbf{p}}^j \right\rangle\right], \qquad [3b]$$

where we have used sum convention for Cartesian indexes, $D_{ij}(\mathbf{k}) := \delta_{ij} - k_i k_j / k^2$ are the components of the projection tensor, $M_{njl}(\mathbf{k}) := -(\mathrm{i}/2)(k_j D_{nl}(\mathbf{k}) + k_l D_{nj}(\mathbf{k}))$, and we have omitted all time arguments for simplicity. The Ekman term (proportional to α) either injects ($\alpha < 0$) or dissipates ($\alpha > 0$) energy into/from the system with a rate proportional to $E_{\mathbf{k}}$. The other linear terms are also responsible for either local energy injection (Γ_0 term) or dissipation (Γ_2 term). The nontrivial dynamics of Eq. **1** result from the nonlinear terms, i.e., advection term and cubic nonlinearity. They couple different wave numbers and provide a flow of energy in spectral space that (on average) balances the local injection or dissipation. The different terms in Eq. **2**, obtained

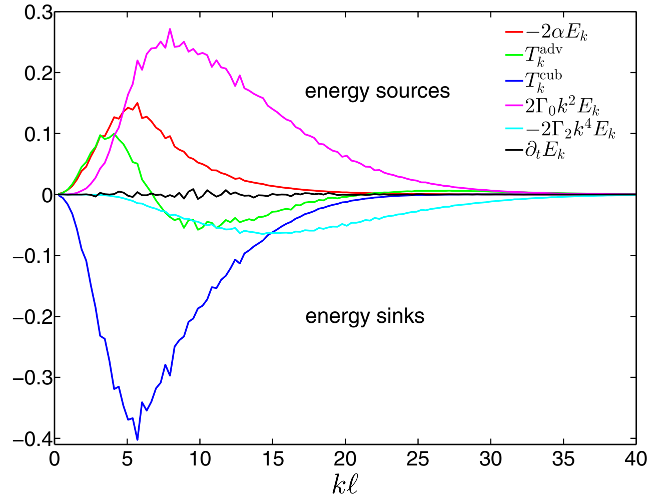

Fig. 2. Spectral form of the different terms in Eq. **2** in the statistically stationary state (time averaged): red, Ekman term; green, advective nonlinearity T_k^{adv}; dark blue, cubic interaction T_k^{cub}; magenta, k^2 injection; light blue, k^4 dissipation; black, time average of the left-hand side. A positive contribution means that at these wave numbers the corresponding term acts as an energy source, and a negative value indicates an energy sink. We see that the nonlinear terms change their character, depending on the scale under consideration. At large and intermediate scales, however, the cubic nonlinearity is always dissipative. Additionally, the Ekman term can provide energy injection or dissipation, depending on the sign of α. For the simulation presented here the latter was set to $\alpha\tau = -1$; i.e., it represents an additional energy source.

from a numerical solution of Eq. **1**, are shown in Fig. 2. We have averaged over nearly 10,000 time steps and (using spherical symmetry) summed over modes with the same absolute value (hence the scalar form of the index k). Note that the advective nonlinearity (green curve) is positive for small k but negative for intermediate k and, thus, transports energy from small to large scales. This inverse energy flow is characteristic of 2D turbulent systems and is due to the constraint of enstrophy conservation (34). In the present context, it takes energy from the intermediate wave numbers where the Γ_0 injection (magenta) is particularly active and transports it to larger scales where it acts as an energy source together with the Ekman term (red) for $\alpha < 0$. At large length scales, those two sources are balanced by the cubic nonlinearity (dark blue) acting as an energy sink for most wave numbers. This energy sink, however, has a nonlinear character that allows it to dynamically adjust its magnitude to the sources for a balance to be reached. Additionally, at large scales the contribution of the cubic interaction is roughly proportional to the energy spectrum E_k. Later, we show that those two features can be derived from a closure approximation for small k.

Spectral Shell Decomposition. To further assess the energy transfer among different length scales, we divide the spectral space into circular shells S_J, $J = 1,2,3,\ldots$ centered at $k = 0$ and complementary to each other. (Details on the shell decomposition are given in *SI Text*, section S2). Moreover, we introduce the projection operator P_J defined as

$$(P_J f)(\mathbf{r}) := \langle f(\mathbf{r})\rangle_J := \sum_{\mathbf{k}\in S_J} f_{\mathbf{k}} \mathrm{e}^{\mathrm{i}\mathbf{k}\cdot\mathbf{r}}. \qquad [4]$$

Such a decomposition will prove useful for analyzing the nonlinear terms. The latter terms represent interactions between different spatial scales and computing the contributions arising from different shells will help us gain physical insights into those interactions, e.g., the degree of locality of the energy transfer. Additionally, examining the symmetry of the shell-to-shell coupling corresponding to the quadratic and cubic nonlinearity will reveal their completely different physical character.

Applying P_J to Eq. **1** leads to an evolution equation for the energy $E_J := \int |\langle \mathbf{v}\rangle_J|^2 \mathrm{d}\Omega/(2V)$ of shell S_J, which reads

$$\frac{\partial E_J}{\partial t} = \sum_{\mathbf{k}\in S_J} \gamma(k)\, |\mathbf{v}_{\mathbf{k}}|^2 + \sum_I \left(T_{IJ}^{\mathrm{adv}} + T_{IJ}^{\mathrm{cub}}\right), \qquad [5]$$

with the advective and cubic nonlinear terms

$$T_{IJ}^{\mathrm{adv}} = -\lambda_0 \sum_{\mathbf{k}} \overline{\langle \mathbf{v}_{\mathbf{k}}\rangle_J} \cdot \mathcal{F}\left\{(\mathbf{v}\cdot\nabla)\langle\mathbf{v}\rangle_I\right\}(\mathbf{k}), \qquad [6a]$$

$$T_{IJ}^{\mathrm{cub}} = -\beta \sum_{\mathbf{k}} \overline{\langle \mathbf{v}_{\mathbf{k}}\rangle_J} \cdot \mathcal{F}\left\{|\mathbf{v}|^2\langle\mathbf{v}\rangle_I\right\}(\mathbf{k}), \qquad [6b]$$

where $\mathcal{F}$ denotes the Fourier transform (*SI Text*, section S1).

The terms T_{IJ}^{adv} and T_{IJ}^{cub} characterize the transfer of energy between shells S_I and S_J. Due to the incompressibility constraint, T_{IJ}^{adv} is antisymmetric with respect to the shell indexes I and J (*SI Text*, section S2); i.e., summing over both indexes gives zero. This shows that (in an incompressible system) the Navier–Stokes nonlinearity neither injects nor dissipates energy but only redistributes it among the different shells S_J. A numerical computation of T_{IJ}^{adv} is shown in Fig. 3*A*. In addition to verifying the antisymmetry, this also illustrates the direction of energy transfer in spectral space. There is a combination of forward and inverse energy flows. At intermediate wave numbers, there is mainly a local forward energy flux; see the areas next to the diagonal in Fig. 3*A*, where red above the diagonal and blue below it indicate a flow from smaller to larger k. Additionally, there is also a nonlocal inverse energy flow dominating at small wave numbers, represented by the smaller side branches in Fig. 3*A*. The green curve in Fig. 2 represents the cumulative effect of the 2D structures seen in Fig. 3*A*. The Navier–Stokes nonlinearity extracts energy from the intermediate wave numbers (negative contribution) and supplies it to both smaller (inverse cascade) and larger (forward cascade) wave numbers. The contribution of the cubic nonlinearity, on the other hand, is symmetric ($T_{IJ}^{\mathrm{cub}} = T_{JI}^{\mathrm{cub}}$) and, therefore, cannot be viewed as a term that simply transfers energy from one shell to another in a conservative manner (*SI Text*, section S2). Because every second-rank tensor can be uniquely decomposed into a symmetric and an antisymmetric part, T_{IJ}^{cub} represents physical processes that are fundamentally distinct from a Navier–Stokes-like energy transfer. It does not redistribute energy between different shells. Instead, it couples different shells, say S_I and S_J, in such a way that the same amount of energy is either produced in both shells or extracted from them. The numerical results displayed in Fig. 3*B* clearly show that the entries of T_{IJ}^{cub} are dominated by the diagonal terms whereas the off-diagonal terms are negligibly small. Note that the curve in Fig. 3*B*, *Inset* resembles closely the blue line in Fig. 2. Moreover, the diagonal entries are negative, indicating the dissipative nature of the cubic nonlinearity. This feature together with the different physical interpretation of the cubic term represents the central result that the shell-to-shell decomposition yields. Both aspects are essential for the cubic interaction and should be captured by a successful closure approximation.

Cubic Damping Term. To make progress beyond a numerical analysis, we seek an approximate solution for the stationary state of the energy spectrum. The analysis is complicated by the fact that the right-hand side of Eq. **2** involves third- and fourth-order velocity correlation functions, $T_{\mathbf{k}}^{\mathrm{adv}}$ and $T_{\mathbf{k}}^{\mathrm{cub}}$. Formulating evolution equations for those gives rise to even higher-order velocity

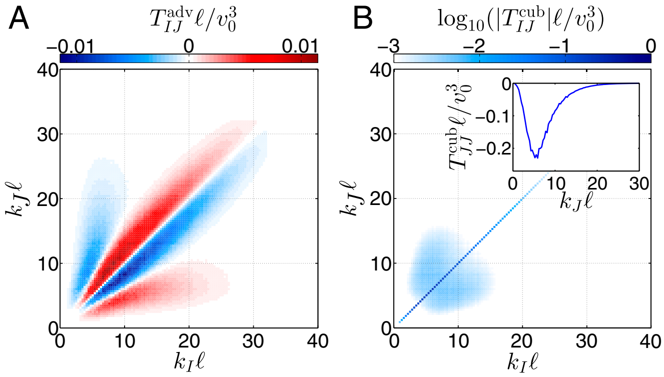

Fig. 3. Numerical computation of the shell-to-shell couplings T_{IJ}^{adv} and T_{IJ}^{cub} as given in Eqs. **6a** and **6b**; all shells have the same width of three times the minimal wave number Δk and a time average over the statistically stationary state has been performed. (*A*) The coupling term T_{IJ}^{adv} due to the advective Navier–Stokes nonlinearity in units of v_0^3/ℓ. It exhibits both forward and backward energy flow in spectral space. At intermediate and large wave numbers there is a local forward flux; see the lobes close to the diagonal. In contrast, for small k, there is an inverse flux nonlocal in spectral space; see the side branches. (*B*) The coupling term T_{IJ}^{cub} due to the cubic nonlinearity in units of v_0^3/ℓ. Note the logarithmic scale. In contrast to the Navier–Stokes term, T_{IJ}^{cub} is symmetric in the shell indexes. In addition, it is almost diagonal, indicating that coupling between different shells is negligible. This shows that at large scales the cubic interaction can be well approximated as a local dissipation term. *Inset* displays only the diagonal entries on a linear scale.

correlations. One way to deal with this "hierarchy" problem is to make approximations at some level (via a "closure relation"), leading to a closed set of equations. Guided by the observation that the statistics of the velocity field at large spatial separations in classical 2D Navier–Stokes turbulence are very close to Gaussian (which we also confirmed numerically for Eq. **1** as explained in *SI Text*, section S3), a natural way to approach the cubic damping term in Eq. **2** is via the quasi-normal approximation (35), also known as the Millionshchikov hypothesis (36). According to it, third-order correlations, e.g., $\langle v^i_{-\mathbf{k}} v^l_{\mathbf{k}-\mathbf{p}} v^j_{\mathbf{p}}\rangle$, are nonzero, and the even-order correlations are approximately sums of products of all possible combinations of second-order correlations (as in Wick's theorem). Defining the scalar correlation function $Q_k(t)$ via $D_{ij}(\mathbf{k})Q_k(t) := \langle v^i_{-\mathbf{k}}(t) v^j_{\mathbf{k}}(t)\rangle$ and using spatial homogeneity and isotropy, one arrives (for a 2D setting) at

$$T_{\mathbf{k}}^{\mathrm{cub}} \approx -\beta Q_k \sum_{\mathbf{p}} \left(2\frac{(\mathbf{k}\cdot\mathbf{p})^2}{k^2p^2}+1\right) Q_p \approx -8\beta\, E_{\mathrm{tot}}\, E_k, \qquad [7]$$

where E_{tot} denotes the total energy of the system; for details of the derivation see *SI Text*, section S3. Hence, the approximation of the cubic damping term in Eq. **2** is directly proportional to the energy spectrum E_k. This resonates with Fig. 3*B*, showing that the diagonal terms are the dominant ones in T_{IJ}^{cub}. Hence, the cubic damping term is of the same form as the linear Ekman damping, however, with a damping rate that is not constant but proportional to the total energy E_{tot} of the system. This captures the nonlinear character of the cubic damping term: It provides a dynamical response at large spatial scales, where an increase of the total energy of the system leads to a stronger dissipation that, in turn, decreases E_k. This nonlinear feature helps to maintain the spectral energy balance and achieve a statistically stationary state. The latter cannot always be attained if $\beta = 0$. Our investigations revealed that in this case there is a critical value for α (necessarily positive) below which the dissipation due to friction is insufficient and cannot balance the energy that accumulates at the large scales as a result of the inverse energy flow in 2D Navier–Stokes systems.

Advective Nonlinearity. In contrast to the cubic damping term, the advective nonlinearity in Eq. **2** produces an expression that involves third-order correlations, meaning that the quasi-normal approximation is not directly applicable. Formulating an evolution equation for the third-order correlation leads to the known hierarchy problem, which here, due to the presence of the cubic term, would be even more convoluted. Such a hierarchical scheme can, nevertheless, lead to a closed system of equations after applying the Millionshchikov hypothesis, but the resulting system of equations is highly complicated and tractable only numerically.

Because our goal here is to arrive at an analytical approximation for the energy spectrum at small wave numbers, we choose a more heuristic approach. As already discussed, the advective nonlinearity redistributes energy only among the different modes. This implies an energy flux in spectral space, defined as $\Pi_k^{\mathrm{adv}} = -\int_0^k T_p^{\mathrm{adv}}\mathrm{d}p$, which is taken to be proportional to the energy E_k at any given scale. The energy corresponding to an eddy of size $\sim 1/k$ scales as $k\,E_k$, which suggests the relation

$$\prod_k^{\mathrm{adv}} \propto \omega_k\, k\, E_k, \qquad [8]$$

where ω_k is a characteristic frequency that may vary with k. Because ω_k is still undetermined, the above relation merely shifts the challenge to finding the function ω_k. However, it suggests a physical interpretation for it. In 2D and 3D Navier–Stokes turbulence this frequency is determined by $\omega_k^2 \sim \int_0^k p^2 E_p \mathrm{d}p$ (35). Physically, $1/\omega_k$ can be viewed as the characteristic distortion time at length scale $1/k$. For the energy cascade in classical turbulence ω_k scales as $k^{2/3}$. Thus, larger eddies have longer eddy turnover times whereas smaller eddies have shorter ones. This implies that over a time period of the order of the eddy turnover time at scale $1/k$ the effects of the larger wave numbers average out due to their faster dynamics. On the other hand, due to their comparatively slower dynamics, the larger length scales (compared with $1/k$) provide a coherent contribution to the average shear rate acting at the scale $1/k$. Given the decrease of E_k with k in the cascade range of Navier–Stokes turbulence, the main contribution to the integral comes from the part of the integrand around $p \sim k$. Thus, most of the shear stems from wave numbers of a magnitude similar to k, which relates to the locality of the classical energy

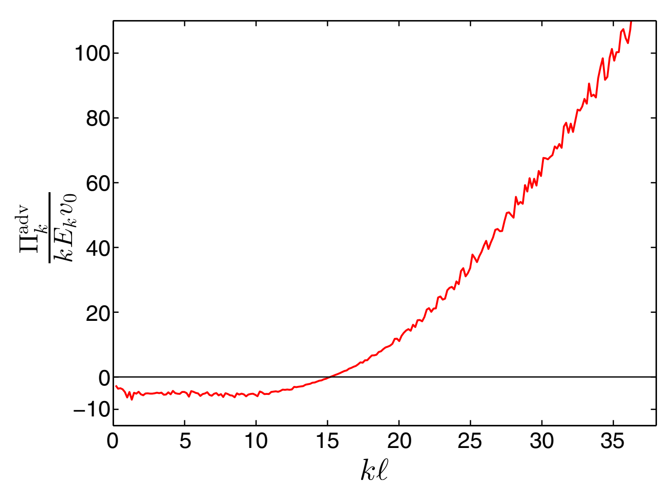

Fig. 4. Numerical computation of the frequency ω_k as a function of k as defined by Eq. **8**. Owing to the positive definiteness of the denominator kE_k, the sign of the function agrees with the sign of the energy flux arising from the advective nonlinearity. Thus, there is evidently an inverse energy flow (negative flux) at large length scales and a forward energy flow (positive flux) at small length scales. Additionally, ω_k is approximately constant at small wave numbers. The numerical simulation was performed with $\alpha\tau = 1$.

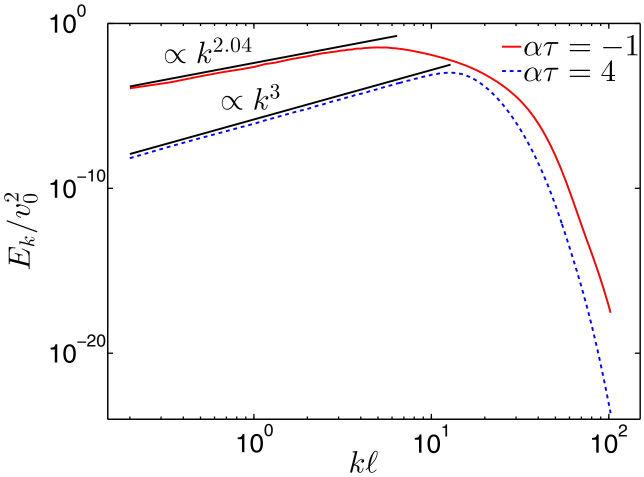

Fig. 5. Time-averaged energy spectrum E_k for two different values of $\alpha\tau$ at the two ends of the parameter domain supporting the turbulent regime, $\alpha\tau = -1$ and $\alpha\tau = 4$. There is a clear power law at large scales and the effect of varying the strength of the Ekman term manifests as a variation of its slope. In general, more intensive energy injection (via the parameter α) leads to a less steep slope of the power law, more energy at each scale, and a peak of the energy spectrum that occurs at smaller wave numbers.

cascade. Eq. **8** together with the integral expression for ω_k given above simplifies the equations and provides a closure that, in the limit of an energy/enstrophy cascade, i.e., constant energy/enstrophy flux, yields the Kraichnan solution for the energy spectrum in the energy/enstrophy inertial range (37). As evident from Fig. 2, however, at large scales there is no range of wave numbers for which the advective nonlinearity is zero; i.e., there is no inertial range. Furthermore, as shown in Fig. 4, the spectral form of the ratio $\Pi_k^{\mathrm{adv}}/(kE_k)$ is constant at large scales, i.e., $\omega_k = \omega_c = \mathrm{const}$, implying that the physics in our case are qualitatively different from what we have in classical Navier–Stokes turbulence, both 2D and 3D. The result that the characteristic frequency is not a function of the local wave number but instead a constant over a wide range in spectral space implies a kind of synchronization of the large-scale structures. Such a synchronization deviates considerably from the classical $\omega_k \propto k^{2/3}$ scaling and requires nonlocal interactions involved in the inverse energy cascade at small k as seen in Fig. 3*A*. In addition, in classical turbulence models large spatial scales are more energetic than smaller ones, giving the former the potential to shear and distort the latter. For Eq. **1**, however, the energy spectrum E_k first increases with k up to some maximum and then decreases again; see the red curve in Fig. 2. Hence, for the spectral region we are interested in, the larger scales are not able to shear the smaller ones. In summary, our investigation of the advective nonlinearity in this model shows that at small wave numbers there is a distinct constant frequency ω_c that controls the energy transfer at large scales. Incorporating this insight into our analysis will provide us with an approximate solution for the energy spectrum at those scales.

Variable Spectral Exponent. In the statistically stationary state, time-averaging Eq. **2** yields zero on the left-hand side,

$$-2\left(\alpha + 4\beta E_{\mathrm{tot}} + \Gamma_0 k^2 - \Gamma_2 k^4\right)E_k - \frac{\mathrm{d}\Pi_k^{\mathrm{adv}}}{\mathrm{d}k} = 0, \qquad [9]$$

where we have already incorporated the result of the quasi-normal approximation for the cubic damping term. Discarding the term proportional to Γ_2 that is negligible at small wave numbers and using Eq. **8** with constant ω_k, we arrive at a differential equation for the energy spectrum E_k, the solution of which reads

$$E_k = \widetilde{E}_0 k^{\delta} \exp\left(-\frac{\Gamma_0}{\lambda_0 \omega_c} k^2\right), \qquad [10]$$

where $\widetilde{E}_0$ is a constant of integration and the exponent is given by $\delta = (2\alpha + 8\beta E_{\mathrm{tot}})/(\lambda_0 \omega_c) - 1$. Eq. **10** shows that at small wave numbers ($k \to 0$) the energy spectrum behaves as a power law. However, the exponent δ of this power law is not universal but depends (directly and indirectly) on various system parameters. Qualitatively, a stronger dissipation, i.e., a positive α and a higher factor of βE_{tot}, will induce a steeper power law. An example is shown in Fig. 5, where the numerical solution of Eq. **1** is presented for two different values of α. In both cases, the system exhibits clear power-law spectra over more than one order of magnitude in wave-number space, and it is evident that our model predicts the correct qualitative dependence of the spectral exponents. A quantitative test of our semianalytical result can be undertaken by carrying out numerical simulations for different values of α. We note in passing that such a parameter scan requires that there are always enough instabilities to drive the turbulence and that statistical homogeneity and isotropy are ensured. The linear growth rate of the most unstable mode equals $-\alpha + \Gamma_0^2/(4\Gamma_2)$, which gives an upper bound on the variation of α once Γ_0 and Γ_2 have been set. On the other hand, the term $-\alpha\mathbf{v}$ in Eq. **1** tries to destroy the statistical isotropy of the system. Thus, the energy injected by the α term must be considerably smaller than that injected by the Γ_2 term, which imposes a lower bound on α. The result from such a parameter scan of the numerical solution of Eq. **1** is displayed in Fig. 6, where every point is obtained by fitting a power law on the left end of the energy spectrum. The data from our investigation show a linear dependence of the slope δ on the parameter α, which agrees with the expression for δ provided by our model. Further numerical simulations indicate that the dependence of the slope on the strength of the cubic interaction β is qualitatively the same but quantitatively much weaker. This can be due to the factor βE_{tot} appearing in δ. Stability analysis shows that for $\lambda_0 = \Gamma_0 = \Gamma_2 = 0$ and $\alpha < 0$ an ordered state arises with a constant velocity field and total system energy $E_{\mathrm{tot}} \propto 1/\beta$. If a similar scaling applies also in the presence of the advective nonlinearity and the other linear

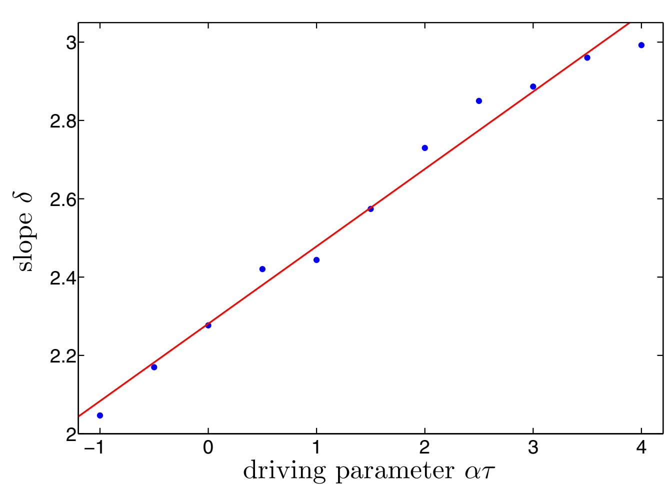

Fig. 6. Variation of the slope of the energy spectrum at small wave numbers with respect to α. The steepness of the power law at large scales varies continuously with the driving parameter in a nearly linear fashion as long as there is a statistically isotropic turbulent regime. The parameter range where this applies derives from the condition that there are enough linear instabilities to sustain the turbulence: i.e., α should not be too large, and the energy injection from the Ekman term should not dominate over the Γ_0 term; i.e., α should not be too negative.

terms, then the product βE_{tot} should exhibit only weak dependence on β.

Summary and Conclusions

In the present work, we investigated the properties of a continuum model describing the turbulent motion of active fluids driven by internal instabilities. In addition to the convective nonlinearity of Navier–Stokes type, the model contains a cubic nonlinearity. Analytical and numerical considerations revealed that at large scales, the latter behaves like an Ekman damping with a frequency that is set by the system self-consistently. The system displays power-law energy spectra even in the absence of an inertial range, but the spectral exponents depend on the system parameters. These properties should be observable in laboratory experiments.

How do these findings fit into a broader perspective on turbulence? In Navier–Stokes turbulence, the dynamics are characterized by an inertial range that is dominated by a single nonlinear term and free of energy sources/sinks, displaying universal properties. Several turbulence models in the literature deviate from this standard picture in that they introduce multiscale forcing and/or damping with a power-law spectrum, thereby removing the inertial range (in a strict sense) (38–40). It can be shown, however, that, in general, this modification really affects the system only at very small or very large scales, i.e., in the asymptotic limit (41). If and only if the power-law exponent is such that the linear forcing/damping rates scale exactly like the nonlinear energy transfer rates, does the forcing/damping affect the entire scale range, inducing nonuniversal behavior (16, 42, 43).

The physical system discussed in this paper is fundamentally different, however. Here, the existence of a second nonlinearity provides additional freedom, such that the system is able to self-organize into such a critical state (characterized by a scale-by-scale balance between linear forcing/damping rates and nonlinear transfer rates), without the need for external fine-tuning. The observed nonuniversal behavior is a natural consequence of this feature. These properties define a new class of turbulence.

ACKNOWLEDGMENTS. V.B. thanks A. Bañón Navarro, M. Oberparleiter, and D. Groselj for helpful discussions. The research leading to these results has received funding from the European Research Council under the European Union's Seventh Framework Programme (FP7/2007-2013)/European Research Council Grant Agreement 277870. It was also supported by the German Excellence Initiative via the program "NanoSystems Initiative Munich" (NIM) and the Deutsche Forschungsgemeinschaft (DFG) in the context of SFB 863 "Forces in Biomolecular Systems" (Project B02).

1. Xu H, et al. (2014) Flight-crash events in turbulence. *Proc Natl Acad Sci USA* 111(21):7558–7563.
2. Perlekar P, Benzi R, Clercx HJH, Nelson DR, Toschi F (2014) Spinodal decomposition in homogeneous and isotropic turbulence. *Phys Rev Lett* 112(1):014502.
3. Kolmogorov AN (1941) The local structure of turbulence in incompressible viscous fluid for very large Reynolds number. *Dokl Akad Nauk SSSR* 30:299–303.
4. Wensink HH, et al. (2012) Meso-scale turbulence in living fluids. *Proc Natl Acad Sci USA* 109(36):14308–14313.
5. Sokolov A, Aranson IS (2012) Physical properties of collective motion in suspensions of bacteria. *Phys Rev Lett* 109(24):248109.
6. Zhou S, Sokolov A, Lavrentovich OD, Aranson IS (2014) Living liquid crystals. *Proc Natl Acad Sci USA* 111(4):1265–1270.
7. Dombrowski C, Cisneros L, Chatkaew S, Goldstein RE, Kessler JO (2004) Self-concentration and large-scale coherence in bacterial dynamics. *Phys Rev Lett* 93(9):098103.
8. Thampi SP, Golestanian R, Yeomans JM (2013) Velocity correlations in an active nematic. *Phys Rev Lett* 111(11):118101.
9. Thampi SP, Golestanian R, Yeomans JM (2014) Vorticity, defects and correlations in active turbulence. *Philos Trans A Math Phys Eng Sci* 372(2029):20130366.
10. Chen X, Dong X, Be'er A, Swinney HL, Zhang HP (2012) Scale-invariant correlations in dynamic bacterial clusters. *Phys Rev Lett* 108(14):148101.
11. Aditi Simha R, Ramaswamy S (2002) Hydrodynamic fluctuations and instabilities in ordered suspensions of self-propelled particles. *Phys Rev Lett* 89(5):058101.
12. Thampi SP, Golestanian R, Yeomans JM (2014) Active nematic materials with substrate friction. *Phys Rev E Stat Nonlin Soft Matter Phys* 90(6):062307.
13. Stresing R, Peinke J, Seoud RE, Vassilicos JC (2010) Defining a new class of turbulent flows. *Phys Rev Lett* 104(19):194501.
14. Elmegreen BG, Scalo J (2004) Interstellar turbulence I: Observations and processes. *Annu Rev Astron Astrophys* 42:211–273.
15. Görler T, Jenko F (2008) Scale separation between electron and ion thermal transport. *Phys Rev Lett* 100:185002.
16. Görler T, Jenko F (2008) Multiscale features of density and frequency spectra from nonlinear gyrokinetics. *Phys Plasmas* 15:102508.
17. Bratanov V, Jenko F, Hatch DR, Wilczek M (2013) Nonuniversal power-law spectra in turbulent systems. *Phys Rev Lett* 111(7):075001.
18. Dunkel J, Heidenreich S, Bär M, Goldstein RE (2013) Minimal continuum theories of structure formation in dense active fluids. *New J Phys* 15:045016.
19. Dunkel J, et al. (2013) Fluid dynamics of bacterial turbulence. *Phys Rev Lett* 110(22):228102.
20. LaQuey RE, Mahajan SM, Rutherford PH, Tang WM (1975) Nonlinear saturation of the trapped-ion mode. *Phys Rev Lett* 34:391–394.
21. Cohen BI, Krommes JA, Tang WM, Rosenbluth MN (1976) Non-linear saturation of the dissipative trapped-ion mode by mode coupling. *Nucl Fusion* 16:971–992.
22. Kuramoto Y, Tsusuki T (1974) Reductive perturbation approach to chemical instabilities. *Prog Theor Phys* 52:1399–1401.
23. Kuramoto Y (1978) Diffusion-induced chaos in reaction systems. *Prog Theor Phys Suppl* 64:346–367.
24. Sivashinsky GI (1977) Nonlinear analysis of hydrodynamic instability in laminar flames-I. Derivation of basic equations. *Acta Astron* 4:1177–1206..
25. Sivashinsky GI (1979) On self-turbulization of a laminar flame. *Acta Astron* 6:569–591.
26. Shraiman BI (1986) Order, disorder, and phase turbulence. *Phys Rev Lett* 57(3):325–328.
27. Swift J, Hohenberg PC (1977) Hydrodynamics fluctuations of the convective instability. *Phys Rev A* 15:319–328.
28. Toner J, Tu Y, Ramaswamy S (2005) Hydrodynamics and phases of flocks. *Ann Phys* 318:170–244.
29. Toner J, Tu Y (1998) Flocks, herds and school: A quantitative theory of flocking. *Phys Rev E Stat Phys Plasmas Fluids Relat Interdiscip Topics* 58:4828–4858.
30. Marchetti MC, et al. (2013) Hydrodynamics of soft active matter. *Rev Mod Phys* 85:1143–1189.
31. Gioia G, Chakraborty P (2006) Turbulent friction in rough pipes and the energy spectrum of the phenomenological theory. *Phys Rev Lett* 96(4):044502.
32. Tran T, et al. (2010) Macroscopic effects of the spectral structure in turbulent flows. *Nat Commun* 6:438–441.
33. Kraichnan RH (1967) Inertial ranges in two-dimensional turbulence. *Phys Fluids* 10:1417–1423.
34. Fjørtoft R (1953) On the changes in the spectral distribution of kinetic energy for two-dimensional, non-divergent flow. *Tellus* 5:225–230.
35. Monin AS, Yaglom AM (1975) *Statistical Fluid Mechanics* (MIT Press, Cambridge, MA).
36. Millionshchikov MD (1941) Theory of homogeneous isotropic turbulence. *Dokl Akad Nauk SSSR* 32:611–614.
37. Kraichnan RH (1971) Inertial-range transfer in two- and three-dimensional turbulence. *J Fluid Mech* 47:525–535.
38. Sain A, Manu, Pandit R (1998) Turbulence and multiscaling in the randomly forced Navier-Stokes equation. *Phys Rev Lett* 81:4377–4380.
39. Biferale L, Lanotte AS, Toschi F (2004) Effects of forcing in three-dimensional turbulent flows. *Phys Rev Lett* 92(9):094503.
40. Vassilicos JC (2015) Dissipation in turbulent flows. *Annu Rev Fluid Mech* 47:95–114.
41. Terry PW, et al. (2012) Dissipation range turbulent cascades in plasmas. *Phys Plasmas* 19:055906.
42. Nam K, Ott E, Antonsen TM, Jr, Guzdar PN (2000) Lagrangian chaos and the effect of drag on the enstrophy cascade in two-dimensional turbulence. *Phys Rev Lett* 84(22):5134–5137.
43. Boffetta G, Cenedese A, Espa S, Musacchio S (2005) Effects of friction on 2D turbulence: An experimental study of the direct cascade. *Europhys Lett* 71(4):590.
44. Gottlieb D, Orszag SA (1977) *Numerical Analysis of Spectral Methods: Theory and Applications* (SIAM, Philadelphia).
45. Cox SM, Matthews PC (2002) Exponential time differencing for stiff systems. *J Comput Phys* 176:430–455.
46. Kassam AK, Trefethen LN (2005) Fourth-order time stepping for stiff PDES. *SIAM J Sci Comput* 26:1214–1233.
47. Canuto C, Hussaini MY, Quarteroni A, Zang ThA (2011) *Spectral Methods: Fundamentals in Single Domains* (Springer, Berlin), 4th Ed.